Research Square

Preprints are preliminary reports that have not undergone peer review.
They should not be considered conclusive, used to inform clinical practice,
or referenced by the media as validated information.

High-performance supercapacitor electrode material based on anthraquinone organic molecules

Maotang Hua
Gansu Institute of Coalfield Geology
Shuya Ji
Lanzhou University of Arts and Science
Shanshan Li
lishsh130@163.com

Lanzhou University of Arts and Science
Yi Zhou
Lanzhou University of Arts and Science
Jianghao Zhou
Lanzhou University of Arts and Science
Jie Li
Lanzhou University of Arts and Science
Yaming Wang
Lanzhou University of Arts and Science
Jinxue Yao
Lanzhou University of Arts and Science
Shoujun Lai
Lanzhou University of Arts and Science

Research Article

Keywords: Organic molecular electrode, Graphene network structure, Non-covalent modification, Supercapacitor

Posted Date: November 18th, 2026

DOI: https://doi.org/10.21203/rs.3.rs-11606764/v1

License: This work is licensed under a Creative Commons Attribution 4.0 International License.
Read Full License

Additional Declarations: No competing interests reported.

High-performance supercapacitor electrode material based on anthraquinone organic molecules

Maotang Hua[1], Shuya Ji[2], Shanshan Li[2]*, Yi Zhou[2], Jianghao Zhou[2], Jie Li[2], Yaming Wang[2], Jinxue Yao[2], Shoujun Lai[2]

1.Gansu Institute of Coalfield Geology, Lanzhou, Gansu 730000, China

2.College of Chemical Engineering, Lanzhou University of Arts and Science, Lanzhou, Gansu 730010, China;

*E-mail: lishsh130@163.com

Abstract: Organic electrode materials, with their high theoretical specific capacity, structural diversity, chemical tunability, low cost and environmental benignity, are consequently favorable candidates for electrochemical energy storage. Herein, we propose a 1-aminoanthraquinone (1-AAQ) based organic molecule electrode engineered to improve energy storage efficiency. Non-covalent π-π interactions enable the immobilization of 1-AAQ molecules onto reduced graphene oxide (rGO) in the system. With a specific capacitance of 327.7 F g^{-1} (1 A g^{-1}), the optimized 1-AAQ-rGO composite maintains a capacitance of 81.5% after 10000 cycles, clearly demonstrating robust cycling performance. To construct an asymmetric supercapacitor (ASC), the positive electrode is fabricated by synergistically integrating benzo[1,2-b:4,5-b']dithiophene-4,8-dione (BDTD) with rGO. The ASC based on 1-AAQ-rGO//BDTD-rGO operates at 1.4 V, delivering an energy density of 18.5 Wh kg^{-1} at a power density of 700 W kg^{-1}. The device preserves 89% capacitance retained after 5000 cycles (5 A g^{-1}). Via empirical substantiation, two ASCs connected in series power 42 LED bulbs. Overall, this work highlights the role of π-π interactions in concurrently boosting capacitance and cyclability, providing a viable route for designing high-performance hybrid supercapacitors.

Keywords: Organic molecular electrode; Graphene network structure; Non-covalent modification; Supercapacitor

1. Introduction

As the continuous expansion of the global economy and the mounting demand for energy supplies, the performance requirements for energy storage systems in portable electronics and electric vehicles have become increasingly stringent[1,2]. There are a lot of innovations in fuel cells, batteries, supercapacitors (SCs)[3-5]. Among these, SCs have garnered tremendous research interest on account of their exceptional power density, durable cyclic stability, and eco-friendly characteristics. Possessing great applicability in sophisticated electrochemical energy storage architectures, supercapacitors are regarded as favorable alternatives to be implemented in portable electronic devices, electric transportation systems, as well as standby power facilities. Nevertheless, the comparatively inferior energy density of SCs remains a formidable bottleneck that limits their widespread practical implementation. Consequently, there is an urgent demand for electrode materials that combine high energy density with cost-effectiveness, long-term durability, and eco-friendliness[6,7].

To address this demand, extensive research has been conducted on various pseudocapacitive electrode materials, including transition metal oxides, sulfides, conductive polymers, hydroxides, nitrides, and electrochemically active organic molecules, all of which are capable of delivering substantially enhanced capacitance and energy density through Faradaic redox reactions[8,9]. Among these candidates, organic molecular electrode materials have garnered particular interest by virtue of their low expense, environmental benignity, high theoretical capacity, rich redox chemistry, and excellent electrochemical reversibility. Changing the functional groups and

molecular architectures can improve the electrochemical characteristics. For example, the introduction of different substituents can shift the redox peak potentials toward either more positive or more negative regions, thereby enabling precise control over the operating voltage of the corresponding electrodes[10]. Quinone derivatives, in particular, have surface as promising electrode materials owing to their strong redox activity, high capacitance, and outstanding reversibility, and have undergone intensive exploration targeting electrochemical energy storage implementations[11,12].

Despite these advances, the practical application of quinone-based electrodes remains hindered by several critical challenges, among which their intrinsically low electronic conductivity is the most prominent, severely limiting their electrochemical performance. To overcome this limitation, one effective strategy is to incorporate redox-active organic molecules into conductive supporting matrices with high specific surface areas, thereby enabling efficient electron transport and enhanced utilization of active sites[13,14]. In this context, graphene has emerged as an ideal conductive scaffold by virtue of its remarkable electronic conductivity, large specific surface area, and superior electrochemical double-layer capacitance[15]. Moreover, to mitigate the intrinsic restacking tendency of graphene sheets, conductive polymers and organic molecules have been integrated into graphene-based frameworks[8,16]. Among the various functionalization approaches, non-covalent modification has proven particularly advantageous, as it preserves the intrinsic conjugated structure and electronic properties of graphene while enabling stable immobilization of redox-active species through interactions such as hydrogen bonding and π-π stacking[17].

Nevertheless, despite these encouraging developments, three key issues remain insufficiently addressed and warrant further investigation. First, the specific capacitance and cycle life performance of most quinone-graphene composites reported to date are still unsatisfactory for practical applications, largely due to the limited loading and poor dispersion of quinone molecules on the graphene surface[18]. Second, the rational design of quinone molecular structures to maximize the synergistic effects with graphene has not been systematically explored[19]. Third, the full potential of such composites in asymmetric supercapacitor configurations has yet to be thoroughly investigated[20].

In this work, an electrode constructed from quinone-based molecules was fabricated, where 1-AAQ was immobilized onto rGO via intense π-π stacking interactions. While a redox center from 1-AAQ is implanted in the rGO structure, intense π-π interactions between 1-AAQ and rGO facilitate charge transfer during the Faradaic reactions. The well-defined hierarchical porous network further facilitates rapid ion penetration into the electrode. In the three-electrode test setup, the 1-AAQ-rGO achieves a specific capacitance of 327.7 F g^{-1} (1 A g^{-1}), and retains 81.5% after 10,000 cycles at 5 A g^{-1}. Meanwhile, the positive electrode fabricated from the BDTD-rGO composite exhibited a Faradaic response at around 0.31 V. Benefiting from the excellent matching of the negative and positive electrodes, the ASC delivers an energy density of 18.5 Wh kg^{-1} at 700 W kg^{-1}, revealing the great potential for energy storage applications. The successful lighting up of 42 LED bulbs via two series-

connected ASC devices highlights the significant potential of aminoanthraquinone functionalized graphene for creating long-lasting all-carbon energy storage devices.

2. Experimental

2.1 Preparation of 1-AAQ-rGO

Graphene oxide (GO) was produced using Hummers' method[21]. First, ultrasonication was applied to achieve dissolution of 0.16 g of 1-aminoanthraquinone (1-AAQ) in 32 mL of N,N-dimethylformamide (DMF). Afterwards, 32 mL of a 2 mg mL^{-1} GO dispersion was incorporated, and the mixture underwent ultrasonication for 1 h. The mixture was then hydrothermally treated at 180 °C for 12 h and allowed to cool naturally to obtain a graphene hydrogel. Ultimately, the hydrogel underwent freeze-drying for 24 h to produce the final product. A schematic of the preparation principle is presented in Fig. 1.

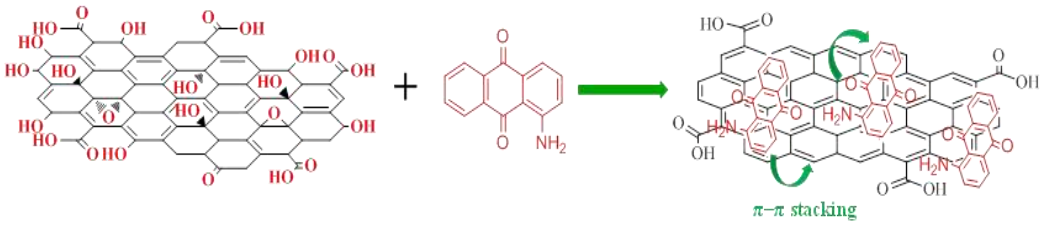


Fig. 1. Schematic of 1-AAQ-rGO synthesis.

3. Results and discussion

3.1. Physical characterization

The surface morphologies of rGO and the 1-AAQ-rGO composite were characterized by scanning electron microscopy (SEM) and transmission electron microscopy (TEM). SEM images (Fig. 2a-d) reveal that both samples retain a typical folded morphology with a three-dimensional hierarchically porous architecture formed

by stacked graphene flakes, indicating that the functionalization with 1-AAQ doesn't damage the overall porous framework of rGO. Such a porous framework and open network act as ion-buffering reservoirs and reduce the diffusion path length of electrolyte ions to penetrate the few-layer graphene sheets, thereby facilitating rapid ion transport[22]. TEM images (Fig. 2e, f), however, reveal a noticeable distinction in the microscopic sheet structure: compared with rGO, 1-AAQ-rGO consists of thinner, more transparent, gauze-like, and wrinkled graphene sheets[23]. This suggests that the adsorption of 1-AAQ onto rGO alleviates the piling of rGO sheets to a certain degree[24], which further optimizes the ion-accessible surface and transport pathways without compromising the intact hierarchical architecture.

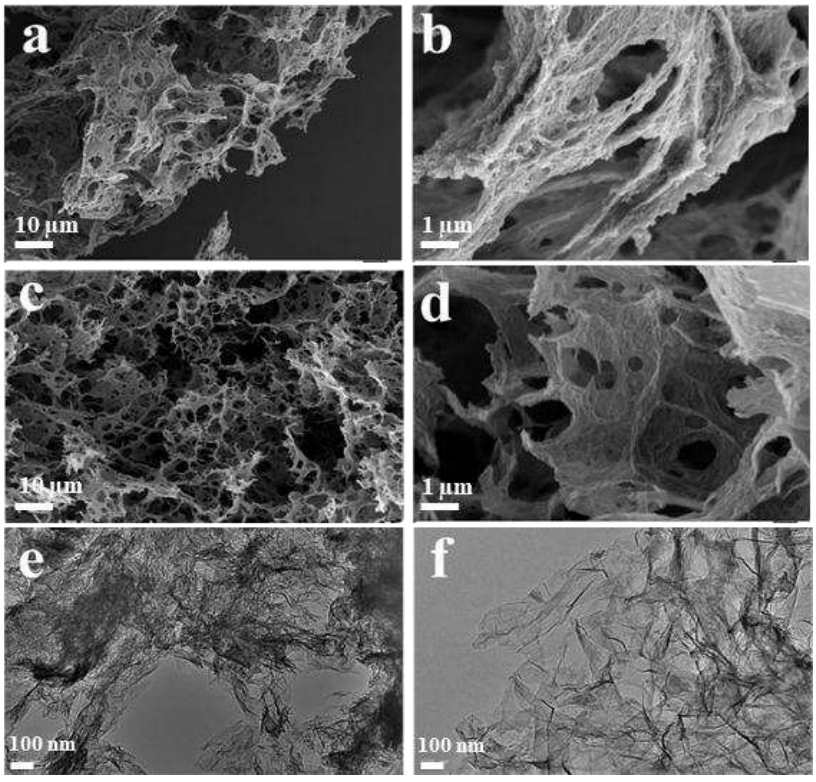


Fig. 2. SEM images of rGO (a, b) and 1-AAQ-rGO (c, d) at different magnifications; TEM images of rGO (e) and 1-AAQ-rGO (f).

Fig. 3a presents the X-ray diffraction (XRD) patterns of rGO and 1-AAQ-rGO. Characteristic (002) diffraction signals appear at 24.9° and 25.5° for rGO and 1-AAQ-rGO, respectively, indicative of interlayer spacings of 0.36 and 0.35 nm[25]. The (002) diffraction peak of 1-AAQ-rGO shifts to a larger angle, which could be assigned to the π-π interaction between 1-AAQ and rGO[26]. As a result of this interaction, the interlayer spacing among graphene sheets is diminished. Moreover, no distinguishable characteristic diffraction peaks corresponding to 1-AAQ can be detected, indicating that 1-AAQ is uniformly dispersed in the composite without forming separate crystalline domains.

Fig. 3b shows the FTIR spectra of pristine 1-AAQ and the 1-AAQ-rGO composite. For pristine 1-AAQ, the absorption bands at approximately 3416 and 3303 cm^{-1} are assigned to the symmetric and asymmetric N-H stretching modes of the amino group, respectively. Other characteristic peaks include the C=O stretching, the C=C vibrations of the benzene ring, a C-N stretching band at 1166 cm^{-1}, and an aromatic C-H bending mode at 697 cm^{-1}. The FTIR spectrum of the 1-AAQ-rGO composite retains all the major characteristic peaks of 1-AAQ. However, the C=C stretching vibration of the aromatic structure shifts slightly to a lower wavenumber (from 1607 to 1571 cm^{-1}). The observed red shift originates from π-π interactions between 1-AAQ and rGO. Since every carbon atom within graphene bears a π electron orbital normal to the graphene plane, allowing π-conjugated molecules such as 1-AAQ to interact with graphene through π-π

stacking[27]. These results indicate that non-covalent π-π interactions tether 1-AAQ molecules to the highly conductive rGO framework.

In Fig. 3c, the Raman spectra of rGO and 1-AAQ-rGO are presented. All samples show two characteristic peaks around 1334 cm^{-1} (D band) and 1596 cm^{-1} (G band)[28]. The intensity ratios (I_D/I_G) serve as a metric for assessing the structural disorder within carbon-based materials[29]. 1-AAQ-rGO has a lower degree of disorder compared to rGO (I_D/I_G: 1.05 *vs*. 1.09), indicating that 1-AAQ effectively anchors to the rGO surface and reduces the extent of defects and disarray in the rGO structure.

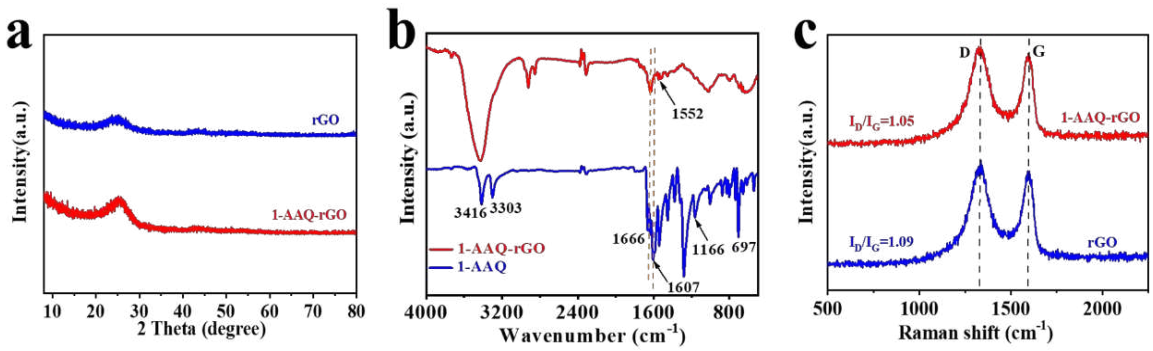


Fig. 3. (a) XRD, (b) FTIR, and (c) Raman spectra of the indicated samples.

The XPS spectra presented in Fig. 4a show that both rGO and 1-AAQ-rGO exhibit main peaks in the C 1s (284.8 eV) and in the O 1s (532.6 eV). Additionally, a new characteristic peak is observed for 1-AAQ-rGO in the N 1s (399.5 eV), indicating that the functionalization of graphene with 1-AAQ was successfully achieved. Deconvolution of the C 1s spectrum of rGO reveals three distinct peaks, which are assigned to C-C/C=C (284.8 eV), C-OH (285.9 eV), and O-C=O (287.9 eV), respectively (Fig. 4b)[30,31]. In comparison, the C 1s spectrum of 1-AAQ-rGO can be resolved into three components at 284.8 eV (C-C/C=C), 286.1 eV (C-O), and 287.8 eV

(C-N/C=O) (Fig. 4c)[32]. The N 1s spectrum of 1-AAQ-rGO shows a binding energy at 399.2 eV, which corresponds to -NH_2 species (Fig. 4d)[33]. These findings provide strong evidence for the successful anchoring of 1-AAQ onto rGO.

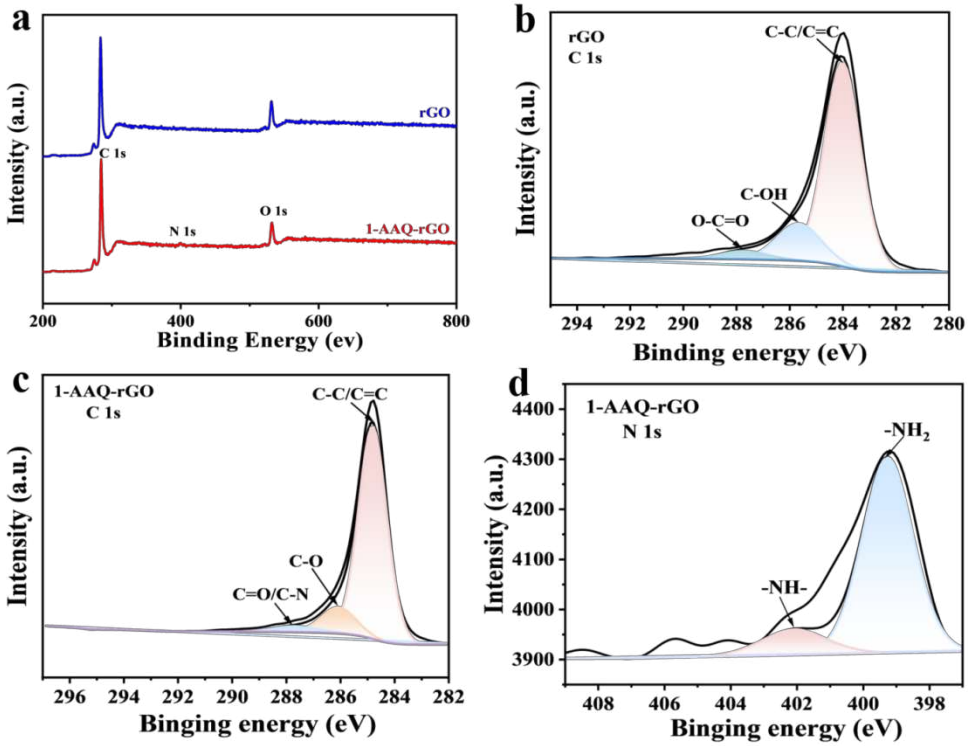


Fig. 4. (a) XPS survey spectra of rGO and 1-AAQ-rGO; (b) C 1s of rGO; (c) C 1s and (d) N 1s of 1-AAQ-rGO.

3.2. Electrochemical measurements

Electrochemical tests of the 1-AAQ-rGO composites were performed in a three-electrode configuration using 1 M H_2SO_4 as the electrolyte over a potential window of -0.4 to 0.6 V. Fig. 5a illustrates the cyclic voltammetry (CV) plots for 1-AAQ, rGO, and 1-AAQ-rGO electrodes at 10 mV s^{-1}. The rGO electrode gives a quasi rectangular curve, clearly manifesting the typical electrical double-layer capacitive (EDLC) feature[34]. Bare 1-AAQ exhibits a weak current signal and negligible capacitive

contribution, which is attributable to its intrinsically poor electronic conductivity. However, owing to the Faradaic reactions derived from the quinonyl/phenolic (O/OH) moieties in 1-AAQ molecules, 1-AAQ-rGO exhibits distinct CV curves, with a pair of redox peaks observed at approximately -0.11/-0.14 V (vs. SCE) (Fig. 5a). The oxidation and reduction peaks of 1-AAQ-rGO are symmetric with a small peak potential separation, suggesting superior electrochemical reversibility[35]. Similarly, Fig. 5b presents the CV curves of 1-AAQ-rGO at 5 to 100 mV s^{-1}. No severe deformation is observed in the curve geometry when elevating the scan rate, indicating excellent rate capability[36].

Fig. 5c shows the galvanostatic charge/discharge (GCD) profiles of the electrodes at 1 A g^{-1}. The GCD curve of the 1-AAQ-rGO electrode exhibits a pair of symmetrical plateaus, indicating that the enhanced capacitance arises from the pseudocapacitive contribution of 1-AAQ. In contrast, the pure 1-AAQ and rGO electrodes show clearly different behavior. The specific capacitance of 1-AAQ-rGO at 1 A g^{-1}, calculated from Equation S1, is 327.7 F g^{-1}, which exceeds that of rGO (194.6 F g^{-1}) and pure 1-AAQ (48 F g^{-1}).

Electrochemical impedance spectroscopy (EIS) was utilized to examine the dynamic characteristics of ion transport across the electrode/electrolyte interface. Fig. 5d presents the Nyquist plots of the 1-AAQ-rGO and rGO electrodes, recorded at a bias potential of 0.2 V. The inset in Fig. 5d shows the expanded high-frequency region; the intercepts of the semicircles with the real axis give Rs=2.57 Ω for rGO and 2.3 Ω for 1-AAQ-rGO. The intercepts of the semicircles with the real axis for 1-AAQ-rGO

indicate a slightly reduced series resistance relative to rGO. This result suggests that the 1-AAQ-rGO composite combines low interfacial resistance, high conductivity, and fast ion-migration kinetics. The electrochemical information derived from EIS measurements matches the trends revealed by CV and GCD characterizations[37].

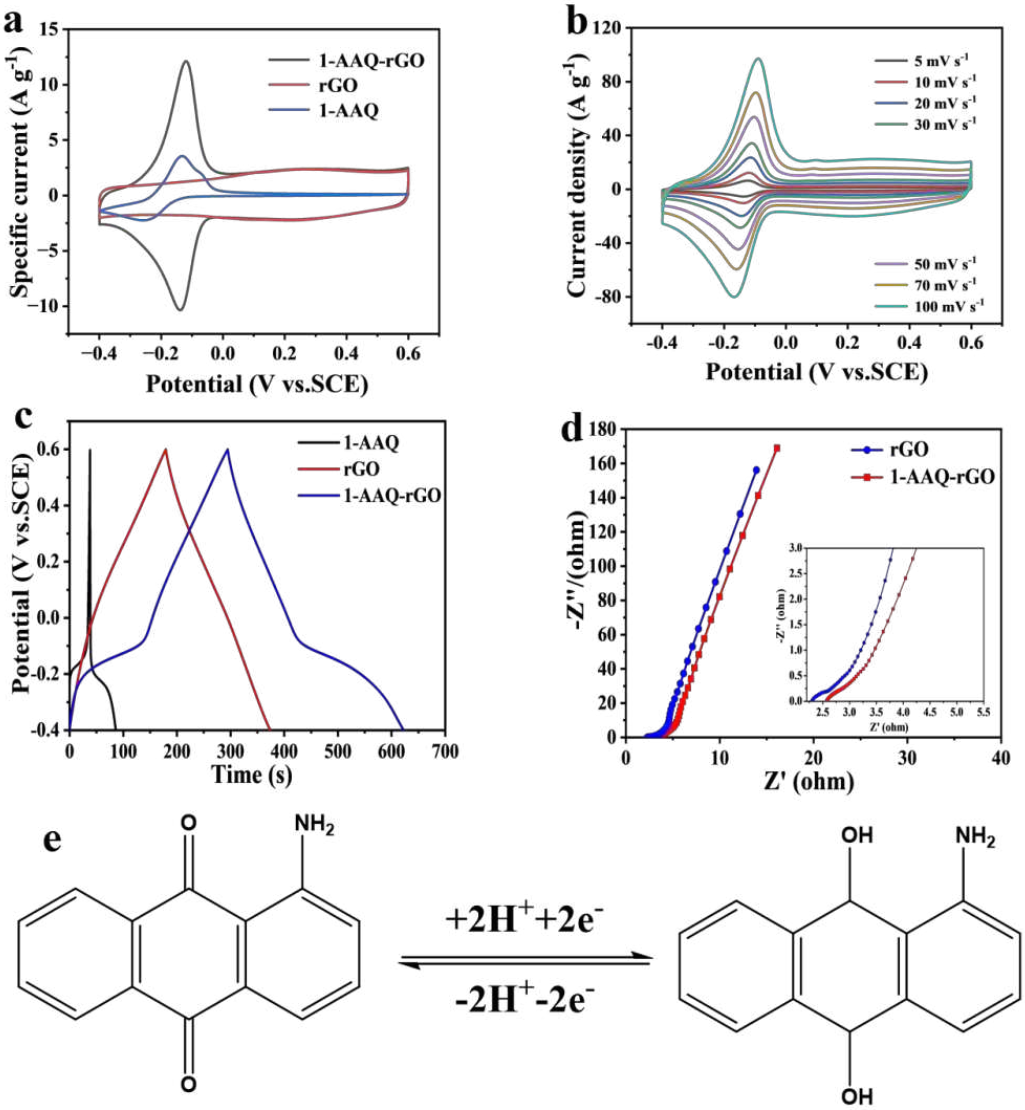


Fig. 5. (a) CV curves at 10 mV s^{-1}; (b) CV curves at different scan rates; (c) GCD curves at 1 A g^{-1}; (d) Nyquist plots; (e) Faradaic reaction of 1-AAQ.

The GCD profiles collected at 1 to 100 A g^{-1} for 1-AAQ-rGO are presented in Fig. 6a and 6b. Remarkably, distinct plateaus during both charging and discharging, together with pronounced symmetry, are retained across the tested current densities, implying

fast and highly reversible electrochemical kinetics[38]. These observations agree well with the CV results. The specific capacitance values of 1-AAQ-rGO at 1-10 A g^{-1} were calculated to be 327.7, 152.6, 102.1, 89.8, 60.2 and 28.5 F g^{-1}, respectively. With a capacitance retention of 79% at 100 A g^{-1}, the 1-AAQ-rGO electrode clearly demonstrates superior rate performance (Fig. 6c). Moreover, Fig. 6d, superior cycling stability is achieved at 5 A g^{-1}, delivering a specific capacitance retention of 81.5% over 10 000 cycles. On the baside of the foregoing experimental finding and discussion, the remarkable electrochemical performance performance of the 1-AAQ-rGO composite can be attributed to the factors listed below: (1) The incorporation of 1-AAQ effectively mitigates the restacking of rGO, thereby shortening ion diffusion pathways and facilitating charge transfer, while simultaneously contributing additional pseudocapacitance through reversible redox reactions[13]. (2) The three-dimensional interconnected porous architecture of the rGO ensures that the electrochemical response of the anchored 1-AAQ molecules is governed by surface-controlled kinetics, which is responsible for the rapid charge-storage response observed in this system[39]. (3) The strong π-π interactions between 1-AAQ and the rGO substrate play a critical role in promoting fast Faradaic reaction kinetics, further bringing about improved overall electrochemical performance[40].

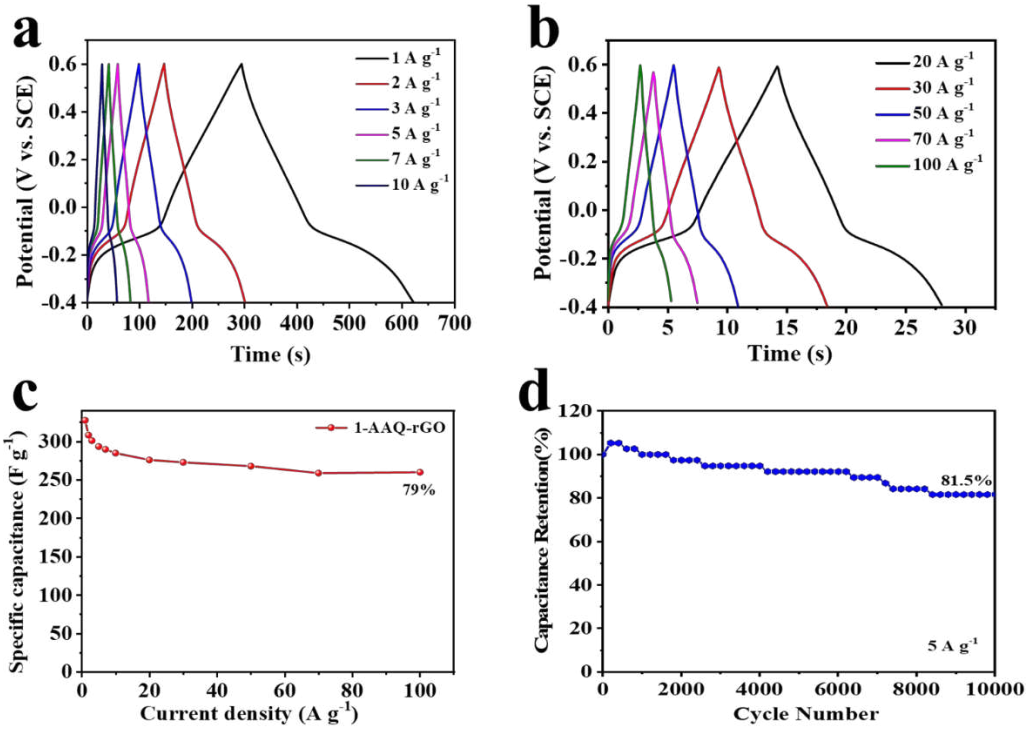


Fig. 6. (a, b) GCD curves; (c) specific capacitance; (d) cycling stability over 10000 cycles.

The differential capacity-potential correlation was interpreted via the formula (dQ/dE=i/v), in which i denotes the current density while v represents the scan rate[41]. For intuitive visualization of redox transitions and charge storage kinetics associated with 1-AAQ-rGO, CV profiles were constructed by plotting differential capacity against potential under diverse scan rates (Fig. 7a). Within 5-100 mV s^{-1}, negligible peak displacement can be observed for 1-AAQ-rGO, which corroborates its favorable electrochemical reversibility[40].

The power-law equation i=a v^{b} provides a means to assess whether surface-controlled or diffusion-limited mechanisms dominate the electrode reactions (a and b denote two constant parameters)[42]. The b-value can be extracted from the slope acquired via the log(i)-log(v) diagram, provides insight into charge-storage mechanisms. The b-value can reveal the charge-storage mechanism: 0.5 corresponds to diffusion-

controlled processes, and 1 to surface-controlled (capacitive) processes[43]. Fig. 7b indicates b-values of 0.931 and 0.914 for the oxidation and reduction peaks of 1-AAQ-rGO, respectively. These values approaching unity confirm the predominance of surface-controlled redox reactions.

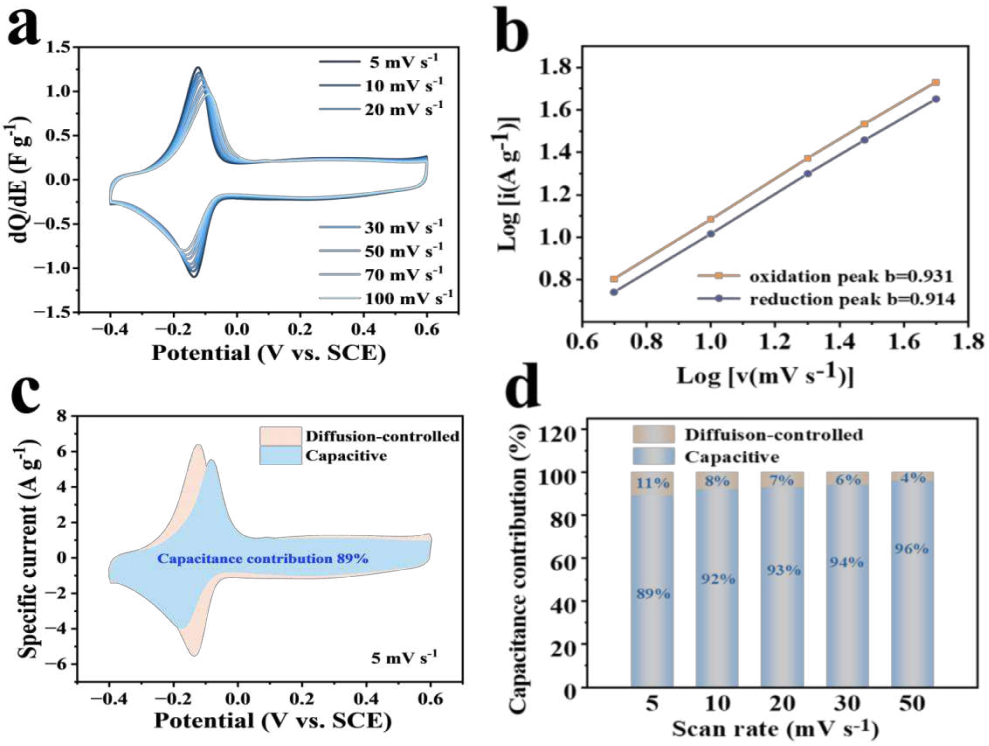


Fig. 7 For 1-AAQ-rGO: (a) differential capacity-potential curves at different scan rates; (b) log(i) vs. log(v) plots; (c, d) capacitive and diffusion contributions.

The capacitive and diffusion-controlled fractions of charge storage were differentiated quantitatively via the expression $i(v)=k_1v+k_2v^{1/2}$, with k_1v and $k_2v^{1/2}$ representing the capacitive and diffusion-controlled terms, respectively[44]. At 5 $mV \cdot s^{-1}$, proportion of 89% of the total capacitance originates from the capacitive contribution (Fig. 7c), evidencing the dominance of capacitive storage. As the scan rate increased to 50 $mV\ s^{-1}$, the capacitive contribution of 1-AAQ- rGO increased from 89% to 96% (Fig. 7d). The observed incremental trend demonstrates pseudocapacitive dominance in the

charge storage process. This finding corroborates the surface-controlled reaction kinetics and swift charge storage properties of the 1-AAQ-rGO electrode.

3.3 Performance of the ASC

The application of the prepared electrodes in supercapacitors was further investigated by ASCs with 1-AAQ-rGO//BDTD-rGO, where 1-AAQ-rGO and the previously studied BDTD-rGO were used as negative and positive electrodes, respectively[45]. Fig. 8a displays the CV profiles of the ASC device, in which a well-defined pair of redox peaks emerges at approximately 0.4 V. The synergy of redox reactions between 1-AAQ-rGO and BDTD-rGO accounts for this observation. Meanwhile, the CV profiles exhibit no notable deformation as high as 100 mV s^{-1}, indicating fast faradaic kinetics for the ASC. The obtained observations are well accordant with the CV characteristics. Moreover, charge-discharge platforms around 0.4 V are observed in GCD profiles of the 1-AAQ-rGO//BDTD-rGO, which are associated with the redox reaction of carbonyl groups, as depicted in Fig. 8b. Nearly ideal symmetry is exhibited by the charge and discharge curves, implying superior electrochemical reversibility. A specific capacitance of 68 F g^{-1} is achieved at 1 A g^{-1}, and 70.4% of the initial capacitance is retained at 10 A g^{-1} (Fig. 8c). Excellent cycling stability is also demonstrated for the ASC, with a high capacitance retention of 89% after 5000 cycles at 5 A g^{-1}. In addition, the Coulombic efficiency remains around 99% throughout the entire cycle (Fig. 8d).

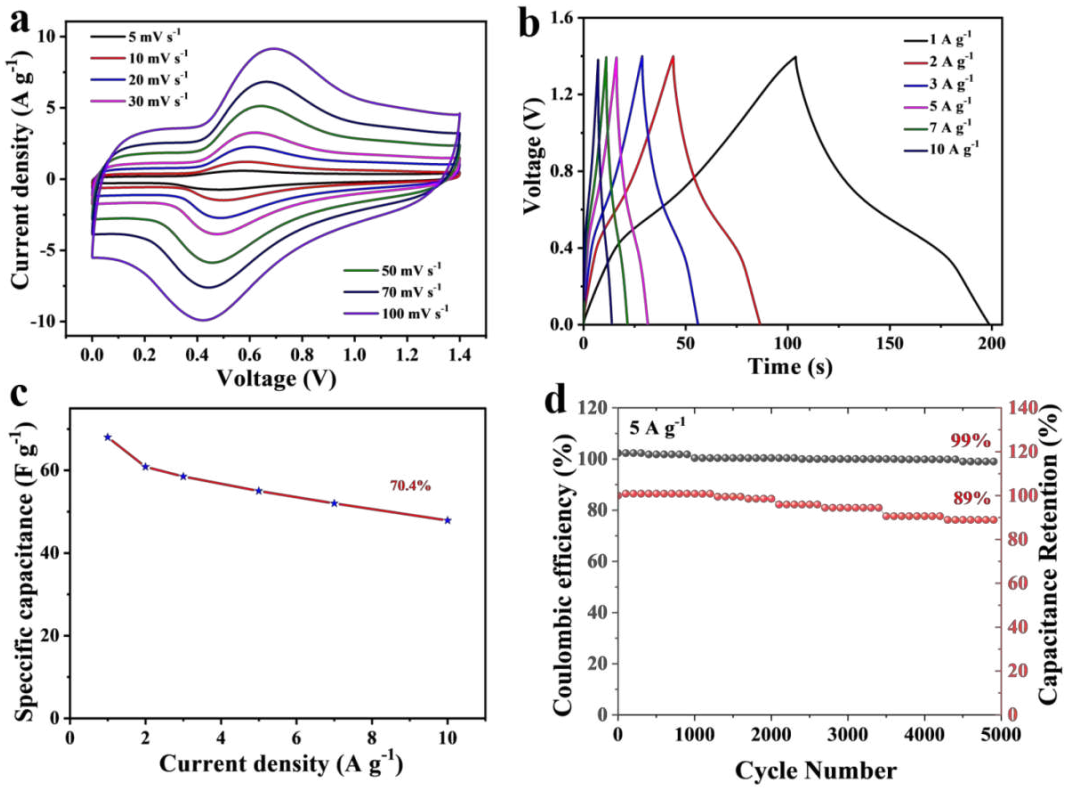


Fig. 8. For the ASC: (a) CV curves; (b) GCD profiles; (c) specific capacitance at various current densities; (d) cycling stability.

Both energy density (E) and power density (P) serve as fundamental criteria for gauging the energy-storage and conversion efficiency of supercapacitors[46]. The energy and power density of the 1-AAQ-rGO//BDTD-rGO ASC can be further evaluated by consulting Fig. 9a, which displays the Ragone plot. Based on equations (S3) and (S4), running at a power density of 700 kW kg^{-1} and a cell voltage of 1.4 V, the supercapacitor attains a maximum energy density of 18.5 Wh kg^{-1}. A superior performance is achieved in this work compared with the earlier investigations listed in Table 1. To evaluate the practical performance of the 1-AAQ-rGO/BDTD-rGO, two tandem ASCs were fabricated to power a light panel containing 42 LEDs (Fig. 9b).

Table 1 Comparison of energy density of 1-AAQ-rGO/BDTD-RGO with reported devices

device	voltage window (V)	power density (W kg^{-1})	energy density (Wh kg^{-1})	Refs
$[EMIM]^+[NO_3]^-$ SC_{OM}	2.0	4000	7.77	47
RGO/DAP-1.5//AC	1.4	350	14.55	48
MNC-900 SC	2.5	128	6.7	49
RGO-ACP_3	1.6	469.24	11.90	50
1-AAQ-rGO//BDTD-rGO	1.4	700	18.5	This work

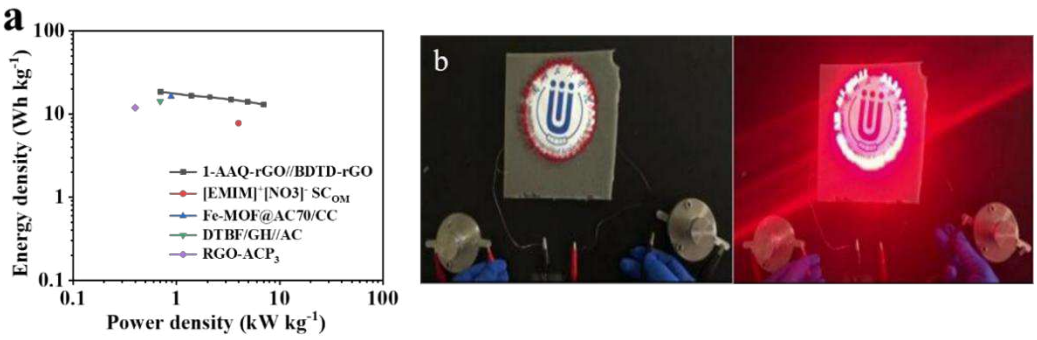


Fig. 9. (a) Ragone plot of the 1-AAQ-rGO//BDTD-rGO, (b) 42 LED bulbs powered by the ASC devices.

4. Conclusion

In summary, a non-covalent π-π functionalization strategy was developed to address the inferior electrical conductivity and limited cycling stability of organic quinone electrodes by anchoring 1-AAQ onto rGO. The resulting 1-AAQ-rGO composite preserves the conjugated structure of graphene while ensuring stable immobilization of redox-active 1-AAQ molecules and efficient charge transfer. The optimized 1-AAQ-rGO electrode delivers a high specific capacitance of 327.7 F g^{-1} at 1 A g^{-1} in 1 M H_2SO_4 and retains 81.5% of its initial capacitance after 10000 cycles at

5 A g^{-1}. When paired with a BDTD-rGO positive electrode, the asymmetric supercapacitor 1-AAQ-rGO//BDTD-rGO achieves an energy density of 18.5 Wh kg^{-1} at a power density of 700 W kg^{-1} and maintains 89% of its capacitance after 5000 cycles at 5 A g^{-1}. It is found that two devices assembled in series can supply power to 42 LED bulbs, demonstrating practical applicability. This work highlights the role of π-π interactions in simultaneously enhancing capacitance and cyclability, offering a viable molecular engineering route for high-performance, sustainable carbon-based supercapacitors.

Credit author contribution statement

Maotang Hua: Methodology, Investigation, Writing-original draft.

Shuya Ji: Investigation, Writing-review & editing.

Shanshan Li: Conceptualization, Supervision, Funding acquisition, Paper revision.

Yi Zhou: Data curation, Validation, Paper revision.

Jianghao Zhou: Investigation, Visualization.

Jie Li: Validation, Formal Analysis.

Yaming Wang: Visualization, Formal Analysis.

Jinxue Yao: Investigation.

Shoujun Lai: Investigation, Funding acquisition.

Conflicts of interest

There are no conflicts of interest to declare.

Acknowledgments

This work was supported by the Natural Science Foundation of Gansu Province (25JRRA1038) and the Regional Science Foundation of the National Natural Science Foundation of China (22267012).

References

[1] Shimizu T, Tanifuji N, Yoshikawa H Azo, compounds as active materials of energy storage systems. Angewandte Chemie International Edition 61 (36), e202206093 (2022). https://doi.org/10.1002/anie.202206093

[2]Liu X, Liu C, Xu S, Cheng T, Wang S, Lai W, Huang W, Porous organic polymers for high-performance supercapacitors. Chem. Soc. Rev 51 (8), 3181-3225 (2022). https://doi.org/10.1039/d2cs00065b

[3] Guan M, Tao W, Xu L, Qin Y, Zhang J, Tan S, Huang M, Zhao B, An asymmetric small-molecule donor enables over 18% efficiency in ternary organic solar cells. Journal of Materials Chemistry A 10 (17), 9746-9752 (2022). https://doi.org/10.1039/d2ta00564f

[4]Xu C, Guan S, Dong X, Huang H, Qi M, Ultratough and Freezing-Tolerant PVA-PAA-PANI Hybrid Hydrogel for Supercapacitors and Flexible Sensors. ACS Sustainable Chem. Eng 11 (41), 14886-14894 (2023). https://doi.org/10.1021/acssuschemeng.3c01164

[5] Younis M, Han J, Yang H, El-Mahdy A, Lee R, Redox-active covalent organic frameworks for supercapacitors: A molecular-level design and integration approach. Renewable Sustainable Energy Rev. 226, 116318 (2026). https://doi.org/10.1016/j.rser.2025.116318.

[6]Jovanovic P, Mirshekarloo M, Aitchison P, Shaibani M, Majumder M, Operando interlayer expansion of multiscale curvedgraphene for volumetrically-efficient supercapacitors. Nat. Commun 16 (1), 8271 (2025). https://doi.org/10.1038/s41467-025-63485-0.

[7]Liu Q, Wang F, Zhang Y, Dong S, Liu Z, Wang L, Feng T, Sui S, Wang Y, Jiang J, Li P, Structural Cement-Based Supercapacitors with Multifunctional Robustness for Energy Storage. Adv. Sci 13 (2), e15769 (2025). https://doi.org/10.1002/advs.202515769

[8] Karuppasamy K, Vikraman D, Hussain S, Santhoshkumar P, Bose R, Sivakumar P, Alfantazi A, Jung J, Kim H, Unveiling the redox electrochemistry of MOF-derived fcc-

NiCo@GC polyhedron as an advanced electrode material for boosting specific energy of the supercapattery. Small 18 (14), 2107284 (2022). https://doi.org/10.1002/smll.202107284

[9] Shi Y, Yang J, Yang J, Wang Zh, Chen Z, Xu Y, Quinone-amine polymer nanoparticles prepared through facile precipitation polymerization as ultrafast and ultralong cycle life cathode materials for lithium-ion batteries. Advanced Functional Materials 32 (21), 2111307 (2022). https://doi.org/10.1002/adfm.202111307

[10] Wu Q, Zhong Y, Chen R, Ling G, Wang X, Shen Y, Hao C, Cu-Ag-C@Ni_3S_4 with core shell structure and rose derived carbon electrode materials: An environmentally friendly supercapacitor with high energy and power density. Ind. Crops Prod 222, 119676 (2024). https://doi.org/10.1016/j.indcrop.2024.119676

[11] Wang X, Pan Y, Wang X, Guo Y, Ni C, Wu J, Hao C, High performance hybrid supercapacitors assembled with multi-cavity nickel cobalt sulfide hollow microspheres as cathode and porous typha-derived carbon as anode. Ind. Crops Prod 189, 115863 (2022). https://doi.org/10.1016/j.indcrop.2022.115863

[12] He Y, Wei Q, An N, Meng C, Hu Zh, Organic small-molecule electrodes: Emerging organic composite materials in supercapacitors for efficient energy storage. Molecules 27 (22), 7692 (2022). https://doi.org/10.3390/molecules27227692

[13] Li S, Zhou Y, Hou G, Ji S, Li X, Li R, Zhang X, Wang J, Lai S, High-energy and long-life all-carbon supercapacitors based on 3-methoxycatechol organic molecular electrodes Electrochim. Acta 541, 147344 (2025). https://doi.org/10.1016/10.1016/j.electacta.2025.147344

[14] Guo Ch, Zhang Y, Yao M, Cao Y, Feng Q, Wang Y, Boosted π-Li Cation Effect in the Stabilized Small Organic Molecule Electrode via Hydrogen Bonding with MXene. ACS Applied Materials & Interfaces 14 (26), 29974-29985 (2022). https://doi.org/10.1021/acsami.2c08366

[15] Barbosa J, Fidalgo-Marijuan A, Dias J, Goncalves R, Salado M, Costa C, Lanceros-Méndez S, Molecular design of functional polymers for organic radical batteries. Energy Storage Mater 60, 102841 (2023). https://doi.org/10.1016/j.ensm.2023.102841

[16] Kang H, Chen Q, Ma Q, Zhang L, Yang Q, Li H, Xie X, Lan Sh, Zhang Ch, Coaxial spiral structural polymer/reduced graphene oxide composite as a high-performance anode for potassium ion batteries. Journal of Power Sources 545, 231951 (2022). https://doi.org/10.1016/j.jpowsour.2022.231951

[17] Georgakilas V, Tiwari J N, Kemp K C, Perman J A, Bourlinos A B, Kim K S, Zboril R, Noncovalent functionalization of graphene and graphene oxide for energy materials, biosensing, catalytic, and biomedical applications. Chemical Reviews 116 (9), 5464-5519 (2016). http://doi.org/10.1021/acs.chemrev.5b00620

[18] Noor N, Baker T, Lee H, Evans E, Angizi S, Henderson J D, Rakhsha A, Higgins D, Redox-Active Phenanthrenequinone Molecules and Nitrogen-Doped Reduced Graphene Oxide as Active Material Composites for Supercapacitor Applications. ACS Omega 9 (9): 10080–10089 (2024). https://doi.org/10.1021/acsomega.3c04836

[19] Karaman C, Bengoa L N, Gonzalez Gil R M, Gómez-Romero P, Quinone Quest: Unraveling electrochemical performance in quinone-anchored 3D graphene architectures for high-energy supercapacitors. Electrochimica Acta 512, 145414 (2025). http://doi.org/10.1016/j.electacta.2024.145414

[20] Hou L, Kong C, Hu Z, Wu B, Han Y, Application of multi-active center organic quinone molecular functionalized graphene in fully pseudocapacitive asymmetric supercapacitors. Nanotechnology 32 (26): 265704 (2021). http://doi.org/10.1088/1361-6528/abf075

[21] Hummers Jr, W. S, Offeman, R. E, Preparation of graphitic oxide. Journal of the american chemical society 80 (6):1339-1339 (1958). https://doi.org/10.1021/ja01539a017

[22]Lee S P, Ali G A M, Assiri M A, Kong K V, Teo E Y L, Chong K F, Pseudocapacitive performance of phenothiazine functionalized graphene aerogel. Applied Surface Science 613, 156069 (2023). http://doi.org/10.1016/j.apsusc.2022.156069

[23] Han J, Xu B, Fang C, Wei J, Li Z, Liu X, Yang Y, Wang Q, Zhang J, Hierarchically Porous Wearable Composites for High Performance Stretchable Supercapacitors. Adv. Sci. 12 (25), 2500835 (2025). http://doi.org/10.1002/advs.202500835

[24] Feng R, Chen Y, Yang L, Du Q, Zhuo K, Ethyl viologen-functionalized reduced g raphene oxide composites for asymmetric ionic liquid-based supercapacitors. Chemica l Engineering Journal 468, 143693 (2023). http://doi.org/10.1016/j.cej.2023.143693

[25] Xiao L, Hu Z, He Y, Jiao L, Lv L, Yin Q, Wei Q, Li Z, Yang Y, Aqueous Electrolyte Asymmetric Supercapacitors Based on the 5-Hydroxyindole Molecule Electrode and MXene with Efficient Energy Storage. ACS Appl. Energy Mater. 6 (1), 68-78 (2023). http://doi.org/10.1021/acsaem.2c02098

[26] Pan B, Bai L, Hu C, Wang X, Li W, Zhao F, Graphene-Indanthrone Donor-π-Acceptor Heterojunctions for HighPerformance Flexible Supercapacitors. Adv. Energy Mater. 10 (18), 2000181 (2020). http://doi.org/10.1002/aenm.202000181

[27] Shi T, Li G, Han Y, Gao Y, Wang F, Hu Z, Cai T, Chu J, Song Z, Oxidized indanthrone as a cost-effective and high-performance organic cathode material for rechargeable lithium batteries. Energy Storage Materials 50, 265-273 (2022). https://doi.org/10.1016/j.ensm.2022.05.013

[28] Wang W, Shen Y, Ma ZH, Wei X, Fan H, Bai Q, High-performance supercapacitors based on self-supporting thick carbon electrodes from renewable biomass wood. Sustainable Materials and Technologies 40, e00824 (2024). http://doi.org/10.1016/j.susmat.2024.e00824

[29] Wang C, Zhou Z, Tian Q, Cao X, Wu Y, Liu S, Wang J, Electropolymerized 1,10-phenanthroline as the electrode material for aqueous supercapacitors. Chem. Eng. 433, 134483 (2022). http://doi.org/10.1016/j.cej.2021.134483

[30] Jana M, Khanra P, Murmu N, Samanta, P, Lee, J, Kuila, T, Covalent surface modification of chemically derived graphene and its application as supercapacitor

electrode material. Physical Chemistry Chemical Physics 16 (16), 7618-7626 (2014). http://doi.org/10.1039/c3cp54510e

[31] Salman M, Chu X, Huang T, Cai S, Yang Q, Dong X, Karthikeyan G, Gao C, Functionalization of wet-spun graphene films using aminophenol molecules for high performance supercapacitors. Materials Chemistry Frontiers 2 (12), 2313-2319 (2018). http://doi.org/10.1039/c8qm00260f

[32] Zhang Y, Liu K, Liu X, Ma W, Li S, Wang J, Fan S, Functionalization of partially reduced graphene oxide hydrogels with 2-Aminopyridine for high-performance symmetric supercapacitors. Journal of Materials Science: Materials in Electronics 32 (14), 18728-18740 (2021). http://doi.org/10.1007/s10854-021-06392-6

[33] Li L, Song B, Maurer L, Lin Z, Lian G, Tuan C, Moon K, Wong C, Molecular engineering of aromatic amine spacers for high-performance graphene-based supercapacitors. Nano Energy, 21, 276-294 (2016). http://doi.org/10.1016/j.nanoen.2016.01.028

[34] Shi M, Peng Ch, Zhang X, A Novel Aqueous Asymmetric Supercapacitor based on Pyrene-4, 5, 9, 10-Tetraone Functionalized Graphene as the Cathode and Annealed Ti_3C_2Tx MXene as the Anode.Small 19 (25), 2301449 (2023). http://doi.org/10.1002/smll.202301449

[35]Wu Q, Sun Y, Bai H,Shi G, High-performance supercapacitor electrodes based on graphene hydrogels modified with 2-aminoanthraquinone moieties. Physical Chemistry Chemical Physics 13 (23), 11193-11198 (2011). https://doi.org/10.1039/c1cp20980a

[36] João P, Fernando C, João I, Rodolfo C, Rafael V, Cesar J.B, Leonardo M, Hudson Zanin, Best practices for electrochemical characterization of supercapacitors. Journal of Energy Chemistry 80, 265-283 (2023). http://doi.org/10.1016/j.jechem.2022.12.034

[37] Muhamad Y, Bashir A, Muaz A, Md. Emdad, Md. Abdul, Turki N, Qasem A, Understanding the behavior of supercapacitor materials via electrochemical impedance spectroscopy: a review, Chem. Rec 24 (5), e202400007 (2024). https://doi.org/10.1002/tcr.202400007

[38] Liu T, Baskoro F, Yang M, Chen L, Sumboja A, Yen H, Kung Y, Electroactive Anthraquinone-Grafted Reduced Graphene Oxide as a Versatile Electrode for

Affordable Supercapacitors and Lithium-Ion Batteries. ACS Applied Energy Materials 9 (2), 782-793 (2026). https://doi.org/10.1021/acsaem.5c02869

[39] Wei Q, Meng C, Xiao L, He Y, Yin Q, Zhou Y, Song S, Qiang R, Yang Y, Li Z, Hu Z, Asymmetric supercapacitors based on 1,10-phenanthroline-5,6-dione molecular electrodes paired with MXene. ChemSusChem 17 (6), e202301370 (2023). https://doi.org/10.1002/cssc.202301370

[40] Zhou Y, Li S, Wu J, Li R, Ji S, Zhao W, Zhou J, Li J, High-Performance Asymmetric Supercapacitors Based on 1, 2-Naphthoquinone Organic Molecular Electrodes. Energy & Fuels 40 (18), 10211-10222 (2026). https://doi.org/10.1021/acs.energyfuels.6c00501

[41] Zhang Z, Li W, Chou S, Han C, Liu H, Dou S, Effects of carbon on electrochemical performance of red phosphorus (P) and carbon composite as anode for sodium ion batteries. Journal of Materials Science & Technology 68, 140-146 (2021). https://doi.org/10.1016/j.jmst.2020.08.034

[42] Shao Y, EI-Kady M F, Sun J, Li Y, Zhang Q, Zhu M, Wang H, Dunn B, Kaner R B, Design and mechanisms of asymmetric supercapacitors. Chemical reviews 118 (18), 9233-9280 (2018). https://doi.org/10.1021/acs.chemrev.8b00252

[43] He Zh, Gao J, Kong L, Electrode materials of cobaltous fluoride for supercapacitor and electrocatalysis applications. Chemistry-An Asian Journal 18 (6), e202201283 (2023). https://doi.org/10.1002/asia.202201283

[44] Shi Z, Chu W, Hou Y, Gao Y, Yang N, Optimization of redox-active anthraquinone as electrode and electrolyte materials in supercapacitors. Electrochimica Acta 370, 137809 (2021). http://doi.org/10.1016/j.electacta.2021.137809

[45]Li S, Wang X, Hou L, Zhang X, Zhou Y, Yang Y, Hu Z, Graphene hydrogels functionalized non-covalently by fused heteroaromatic molecule for asymmetric supercapacitor with ultra-long cycle life. Electrochimica Acta 317, 437-448 (2019). http://doi.org/10.1016/j.electacta.2019.06.022

[46] Xu Y, Li Q, Guo X, Zhang S, Li W, Pang H, Metal organic frameworks and their composites for supercapacitor application.Journal of Energy Storage 56, 105819 (2022). http://doi.org/10.1016/j.est.2022.105819

[47] Park J, Sun J, Phase-transitional ionogel-based supercapacitors for a selective operation. ACS Applied Materials Interfaces 14 (20), 23375-23382 (2022). http://doi.org/10.1021/acsami.2c02160

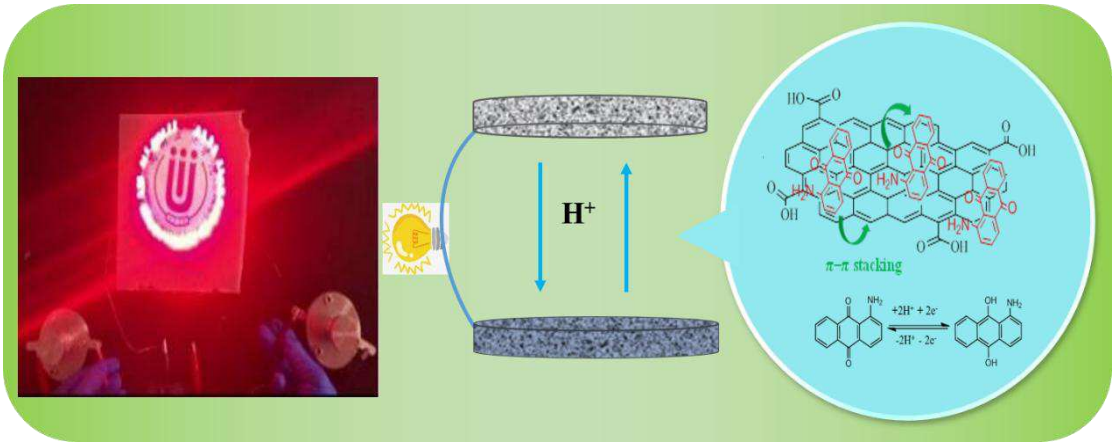
[48] Zhang W, Li Y, Kang H, Yang B, Li Z, Liu H, 2, 6-Diaminopyridine decorated reduced graphene oxide as integrated electrode with excellent electrochemical properties for aqueous supercapacitors. Electrochimica Acta, 404, 139725 (2022). https://doi.org/10.1016/j.electacta.2021.139725

[49] Liu Y, Huang G, Li Y, Yao Y, Liu Q, Xing B, Jia J, Zhang C, Structural evolution of porous graphitic carbon nanosheets based on quinonyl decomposition for supercapacitor electrodes. Applied Surface Science 537, 147824 (2021). https://doi.org/10.1016/j.apsusc.2020.147824

[50] Wang J, Li Q, Peng Ch, Shu N, Niu L, Zhu Y W, To increase electrochemical performance of electrode material by attaching activated carbon particles on reduced graphene oxide sheets for supercapacitor. Journal of Power Sources 450, 227611 (2020). https://doi.org/10.1016/j.jpowsour.2019.227611

Graphical abstract

An aminoanthraquinone-based organic molecule electrode is developed for efficient energy storage. 1-aminoanthraquinone (1-AAQ) is anchored onto reduced graphene oxide (rGO) via π-π interactions to form an organic molecule electrode (1-AAQ-rGO). Benzo[1,2-b:4,5-b']dithiophene-4,8-dione (BDTD) is combined with rGO as the positive electrode and paired with 1-AAQ-rGO to fabricate an asymmetric supercapacitor (1-AAQ-rGO//BDTD-rGO). The device delivers an energy density of 18.5 Wh kg^{-1} at a power density of 700 W kg^{-1}, with 89% capacitance retention after 5000 cycles at 5 A g^{-1}. Two series-connected devices can power 42 LED bulbs.



Supplementary Files

This is a list of supplementary files associated with this preprint. Click to download.

- SupportingInformation.docx